Journal of Magnetism and Magnetic Materials 656 (2026) 174461

Contents lists available at ScienceDirect

Journal of Magnetism and Magnetic Materials

journal homepage: www.elsevier.com/locate/jmmm

Research article

Effect of spin disorder on the specific loss power of a nanomagnet

A. Michels [a], H. Kachkachi [b,*]

[a] Department of Physics and Materials Science, University of Luxembourg, 162A avenue de la Faiencerie, L-1511 Luxembourg, Grand Duchy of Luxembourg
[b] Laboratoire PROMES CNRS (UPR-8521), Université de Perpignan Via Domitia, Rambla de la Thermodynamique, Tecnosud, 66100 Perpignan, France

ARTICLE INFO

Keywords:
Magnetic hyperthermia
Magnetic nanoparticles
Specific absorption rate
Surface effects

ABSTRACT

Spin non-collinearities in magnetic nanostructures arise from a variety of sources, including structural defects, finite-size effects, boundary or surface effects, Dzyaloshinskii–Moriya exchange coupling, and magnetic vortex formation. While strong forms of spin disorder generally require a numerical treatment, relatively weak non-collinearities induced by surface anisotropy are amenable to the analytical framework of the effective one-spin problem (EOSP). In this work, we exploit this framework to present a qualitative, semi-analytical study of the effect of spin disorder on the specific loss power (SLP) of a single nanomagnet within linear-response theory. Surface-induced spin misalignment mainly manifests as an additional quartic (cubic-symmetry) contribution to the anisotropy energy, parametrized by the ratio $\zeta \equiv K_4/K_2$. We derive a semi-analytical expression for the SLP as a function of ζ by combining the ζ-dependent equilibrium susceptibility and the relaxation rate obtained within Langer's approach. Our results show that, for systems in the slow-relaxation regime, the SLP is enhanced by spin misalignment, predominantly through the increase of the relaxation rate caused by the lowering of the effective energy barrier. Retaining the full Debye factor reveals that for moderate reduced barriers σ, where the system is close to the superparamagnetic regime, the SLP can actually *decrease* with increasing spin disorder. The enhancement is asymmetric with respect to the sign of ζ and depends on the nanomagnet shape (sphere versus cube) through the geometric prefactors in the EOSP mapping.

1. Introduction

Magnetic hyperthermia, the controlled heating of tissue by magnetic nanoparticles (NPs) subjected to an alternating magnetic field, is one of the most promising biomedical applications of nanomagnetism [1–6]. The efficiency of the heating is quantified by the specific loss power (SLP), defined as the electromagnetic power absorbed per unit mass of magnetic material. Within the linear-response theory (LRT), the SLP is directly proportional to the imaginary part of the AC susceptibility [7–11],

$$\mathrm{SLP} = \frac{\mu_0\,\omega}{2\pi}\,H_0^2\,\chi''(\omega), \tag{1}$$

where $\omega = 2\pi f$ is the angular frequency of the AC field of amplitude H_0.

Extensive theoretical work has been devoted to the dependence of the SLP on interparticle dipolar interactions (DI) and on an external DC bias field [3,6,12,13]. However, real nanomagnets are not perfect macrospins: spin non-collinearities are ubiquitous and can be induced by structural defects, finite-size effects, and boundary or surface effects [14–25]. In fact, the disruption of the spin ordering can be significantly more severe when caused by magnetic vortex formation [26–28], spin frustration at interfaces, or antisymmetric Dzyaloshinskii–Moriya (DM) exchange coupling [29,30]. In such cases, the spin texture may be far from a simple canted configuration and a full numerical treatment of the many-spin problem is generally required [31]. The influence of spin disorder on the SLP has received comparatively little attention, despite the fact that non-collinearities are known to strongly modify the effective anisotropy of nanomagnets and, therefore, their magnetization dynamics. A recent step in this direction is the work of Faílde et al. [32], who showed by kinetic Monte Carlo simulations that going beyond the uniaxial-anisotropy description — in particular accounting for cubic anisotropy contributions — can significantly affect the predicted heating performance. A related strand of work addresses the effect of strong, spatially uncorrelated (random) anisotropy on the microwave response of macroscopic ferromagnets [33,34]; this is a physically distinct disorder regime from the weak, coherent surface-induced anisotropy treated here.

Among the various sources of spin misalignment, *surface anisotropy* (SA) is particularly relevant for small magnetic NPs, where the surface-to-volume ratio is large. Importantly, the relatively weak spin misalignment produced by SA — when the surface anisotropy remains moderate

* Corresponding author.
E-mail address: hamid.kachkachi@univ-perp.fr (H. Kachkachi).

https://doi.org/10.1016/j.jmmm.2026.174461
Received 2 April 2026; Received in revised form 29 July 2026; Accepted 29 July 2026
Available online 4 August 2026

compared to the exchange coupling — is amenable to an *analytical* treatment through the effective one-spin problem (EOSP) framework. This makes SA the ideal testing ground for a qualitative study of how spin non-collinearities affect the SLP, while keeping the calculation fully analytical.

The purpose of the present work is therefore to present a qualitative, semi-analytical investigation of the influence of spin disorder on the SLP of an *isolated* nanomagnet (i.e., neglecting DI), taking surface-induced non-collinearities as a concrete and experimentally relevant example. We combine the analytical results for the ζ-dependent equilibrium susceptibility and the relaxation rate derived in Refs. [12,35] to obtain a semi-analytical expression for the SLP as a function of ζ, a parameter that reflects the strength of the surface-induced spin disorder. We stress that, although the present analysis is restricted to the weak-disorder regime captured by the EOSP, the qualitative trends it reveals — in particular the competition between barrier lowering and the Debye dissipation condition — are expected to persist, and likely to be amplified, when stronger forms of spin disorder are present.

2. Model and formalism

2.1. EOSP energy

It has been shown that, for weak-to-moderate surface disorder, the energy of a many-spin nanomagnet (a crystallite) can be mapped onto the *effective one-spin problem* (EOSP) [21–23,36]. More precisely, the EOSP is obtained from the many-spin problem (MSP) under certain conditions regarding the surface anisotropy, which should not be too strong with respect to the exchange coupling, and the particle size, which should not be too small (see Refs. [21–23,36] for details). The EOSP consists of the net magnetic moment

$$\boldsymbol{m} = \frac{\sum_i \boldsymbol{s}_i}{\| \sum_i \boldsymbol{s}_i \|}. \tag{2}$$

with $\|\boldsymbol{s}_i\| = 1$, evolving in an effective energy potential given by

$$\mathcal{H}_{\rm eff} \simeq -k_2 m_z^2 + k_4 \sum_{\alpha=x,y,z} m_\alpha^4. \tag{3}$$

The values and signs of the (effective) coefficients k_2 and k_4 are functions of the atomistic parameters $J, K_{\rm c}, K_{\rm s}$, in addition to the size and shape of the nanomagnet and its underlying crystal lattice [21]. In the following, we will use the dimensionless constants defined by $k_{\rm c} = K_{\rm c}/J$ and $k_{\rm s} = K_{\rm s}/J$, so that k_2 and k_4 are dimensionless.

For a nanomagnet cut out of a simple cubic lattice, we have [22,37]

$$k_2 = k_{\rm c}\frac{N_{\rm c}}{\mathcal{N}}, \quad k_4 \simeq \begin{cases} \kappa \frac{k_{\rm s}^2}{z}, & \text{sphere,} \\ \left(1 - 0.7/\mathcal{N}^{1/3}\right)^4 \frac{k_{\rm s}^2}{z}, & \text{cube,} \end{cases} \tag{4}$$

where z is the coordination number, κ represents a (dimensionless) surface integral, and $N_{\rm c}$ is the number of atoms in the core of the nanomagnet (with full coordination), while $\mathcal{N}$ is the total number of atoms (including both the core and surface). Note that κ was derived in Ref. [22] in the absence of core anisotropy. As shown in Ref. [38], in the presence of the latter, the spin misalignment caused by surface anisotropy does not propagate to the center of the nanomagnet; it is "fended off" by the uniaxial anisotropy in the core which tends to align all spins together. The result of this competition is that k_4 (or κ) is multiplied by the factor $N_{\rm c}/\mathcal{N}$. Likewise, for both the cube and sphere, k_2 may be approximated [36] by the first expression in Eq. (4).

We define the two dimensionless relevant parameters

$$\sigma \equiv \frac{K_2 V}{k_B T}, \qquad \zeta \equiv \frac{K_4}{K_2}, \tag{5}$$

so that σ is the reduced uniaxial anisotropy-energy barrier and ζ measures the relative strength of the surface-induced quartic anisotropy.

The sign and magnitude of ζ depend on the crystal structure, shape, and surface arrangement of the nanomagnet, as was studied in detail by Yanes et al. [21]. For particles cut from a simple cubic (sc) lattice, the effective cubic constant K_4 is negative (i.e., $\zeta < 0$), favoring alignment of the magnetization along the cube edges. In contrast, for particles cut from a face-centered cubic (fcc) lattice, K_4 is positive ($\zeta > 0$), favoring alignment along the cube diagonals [21]. In both cases, $K_4 \propto K_{\rm s}^2$, so ζ is quadratic in the surface anisotropy constant. For elongated particles, there is an additional first-order contribution to the effective uniaxial anisotropy (K_2) that is linear in $K_{\rm s}$ and scales with the surface-to-volume ratio, but the quartic contribution remains proportional to $K_{\rm s}^2$ [21,24]. The EOSP mapping is valid as long as $|\zeta|$ remains below a critical value, estimated numerically to be ∼0.25 for sc and ∼0.35 for fcc lattices [21].

2.2. AC susceptibility within the LRT

In the Debye model, the AC susceptibility of a nanomagnet with oriented uniaxial anisotropy in a longitudinal probing field reads [39–41]

$$\chi(\omega) = \frac{\chi_{\rm eq}}{1 + i\omega/\Gamma_0}, \tag{6}$$

where $\chi_{\rm eq}$ is the equilibrium (static) susceptibility and Γ_0 is the longitudinal relaxation rate. The imaginary part of χ is then

$$\chi'' = \chi_{\rm eq}\frac{\eta_0}{1+\eta_0^2}, \tag{7}$$

with $\eta_0 \equiv \omega/\Gamma_0$. Using Eq. (1), the SLP is

$$\mathrm{SLP} = \frac{\mu_0\,\omega}{2\pi} H_0^2\, \chi_{\rm eq}\frac{\eta_0}{1+\eta_0^2}. \tag{8}$$

We now express $\chi_{\rm eq}$ and Γ_0 as functions of ζ.

2.2.1. Equilibrium susceptibility

For a noninteracting nanomagnet described by the EOSP model in zero DC field, the equilibrium susceptibility in the limit $\sigma \gg 1$ reads [35,42]

$$\chi_{\rm eq}(\sigma,\zeta) = 2\chi_0^{\perp}\,\sigma\,\chi_{\rm free}^{(1)}, \tag{9}$$

with $\chi_0^{\perp} \equiv \mu_0 m^2/(2K_2V)$ and

$$\chi_{\rm free}^{(1)} = \left(1 - \frac{1}{\sigma}\right) + \frac{\zeta}{\sigma}\left(-1 + \frac{2}{\sigma}\right). \tag{10}$$

To linear order in ζ, this can be decomposed as

$$\chi_{\rm eq} = \chi_{\rm eq}^{(0)} + \zeta\,\delta\chi_{\rm eq}, \tag{11}$$

where $\chi_{\rm eq}^{(0)} = 2\chi_0^{\perp}(\sigma - 1)$ is the standard uniaxial result and $\delta\chi_{\rm eq} = 2\chi_0^{\perp}(2/\sigma - 1)$ is the SA correction. Note that $\delta\chi_{\rm eq} < 0$ for $\sigma > 2$, confirming that SA *decreases* the equilibrium susceptibility [35].

2.2.2. Relaxation rate

The relaxation rate of the EOSP nanomagnet in zero field and for $|\zeta| \gtrsim \zeta_{\rm crit}$ is computed within Langer's approach [43–50][1] In the EOSP potential (3), the cubic anisotropy breaks the continuous rotational symmetry around the easy axis and creates four saddle points at the equator. For $\zeta > 0$ and $h = 0$, the saddle points are located at $\theta_{\rm s} = \pi/2$ with $\varphi_{\rm s} = \pi/4 + n\pi/2$ ($n = 0,1,2,3$), while for $\zeta < 0$ they lie at $\varphi_{\rm s} = n\pi/2$ [35]. The overall topology of the energy landscape remains similar for both signs of ζ; what changes is the azimuthal locus of the saddle points and the values of the energy and curvatures thereat. Langer's formula reads [35,50]

$$\tau_{\rm D}\,\Gamma_0 = 4\,\frac{|\nu|}{2\pi}\,\frac{2\sigma(1-\zeta)\,\sin\theta_{\rm s}}{\sqrt{|\mu_1^{(\rm s)}\mu_2^{(\rm s)}|}}\,e^{\Delta E^{(0)}}, \tag{12}$$

[1] The critical value $\zeta_{\rm crit}$ was discussed in Ref. [35].

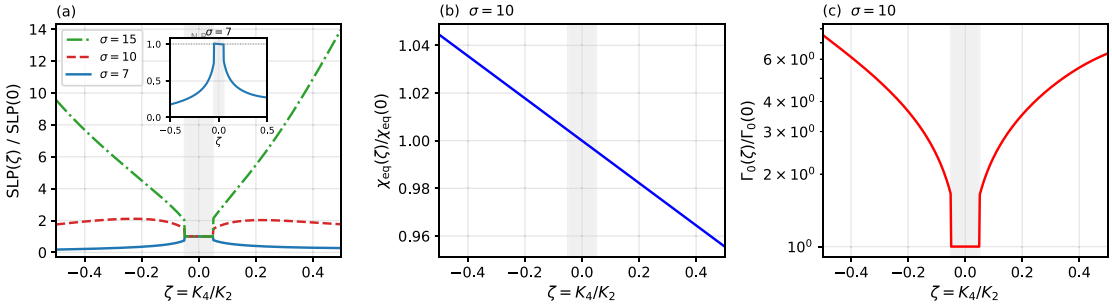

Fig. 1. (a) SLP normalized to its $\zeta = 0$ value as a function of the surface-anisotropy parameter ζ for three values of the reduced barrier σ. The inset magnifies the $\sigma = 7$ curve, which decreases monotonically with $|\zeta|$ (fast-relaxation regime, $\eta_0 < 1$). (b) Equilibrium susceptibility $\chi_{\rm eq}$, normalized to its $\zeta = 0$ value, for $\sigma = 10$. (c) Relaxation rate Γ_0, normalized to its $\zeta = 0$ value, for $\sigma = 10$. The shaded band near $\zeta = 0$ marks the crossover region where Langer's approach is not applicable and the Néel–Brown rate is used, which is independent of ζ. Parameters: $\lambda = 1$, $\tau_0 = 10^{-9}$ s, $f = 100$ kHz, $\mu_0 H_0 = 10$ mT.

where $\tau_{\rm D} = \left(\lambda\gamma H_{\rm K}\right)^{-1}$ is the free diffusion time, $H_{\rm K} = 2K_2V/M_{\rm s}$ is the (uniaxial) anisotropy field, and $\gamma \simeq 1.76\times10^{11}$ (Ts)$^{-1}$ the gyromagnetic ratio.

In Eq. (12), ν is the attempt frequency determined by the eigenvalues $\mu_{1,2}^{(\rm s)}$ of the energy Hessian at the saddle point [35]. The energy barrier is

$$-\Delta E^{(0)} = \begin{cases} \sigma(1-\zeta/4) & \text{for } \zeta > 0, \\ \sigma & \text{for } \zeta < 0. \end{cases} \tag{13}$$

For $\zeta > 0$, the barrier is reduced by $\sigma\zeta/4$ relative to the pure uniaxial value σ, leading to an exponential enhancement of the relaxation rate. Remarkably, for $\zeta < 0$ the energy barrier remains equal to σ and is thus independent of ζ. In this case, the SA contribution enters only through the Kramers prefactor, i.e., through the eigenvalues $\mu_{1,2}^{(\rm s)}$ and the attempt frequency ν. The eigenvalues at the saddle also differ: for $\zeta > 0$, $\mu_1^{(\rm s)} = \sigma(\zeta+2)$ and $\mu_2^{(\rm s)} = -2\sigma\zeta$, while for $\zeta < 0$, $\mu_1^{(\rm s)} = 2\sigma(1+\zeta)$ and $\mu_2^{(\rm s)} = 2\sigma\zeta$ [35]. In the narrow window $|\zeta| < \zeta_{\rm crit}$, the saddle-point structure is too flat for Langer's approach to be valid, and the relaxation rate reduces to the Néel–Brown result [51–53] $\tau_{\rm D}\Gamma_{\rm NB} = (2/\sqrt{\pi})\,\sigma^{1/2}\,e^{-\sigma}$, which is independent of ζ. We note that analytic approximations for the field-dependent relaxation time of nanoparticle systems with uniaxial anisotropy have recently been developed by Davidson et al. [54]; the present work extends the analysis to the case where a quartic term modifies the energy landscape. The general case with both uniaxial and cubic anisotropy, in the presence of a DC field, is also studied in Ref. [35], but here the DC field is ignored for simplicity.

2.3. SLP as a function of ζ

Substituting Eqs. (9)–(12) into Eq. (8), one obtains a semi-analytical expression for the SLP as a function of ζ, σ, λ, and the field parameters ω and H_0. Note that the Debye factor $\eta_0/(1+\eta_0^2)$ in Eq. (8) peaks at $\eta_0 = 1$ and decreases on either side. In the deep slow-relaxation regime $\eta_0 \gg 1$ (large σ), this factor reduces to Γ_0/ω and the SLP grows with Γ_0. Conversely, when σ is only moderate and the system is close to or below the $\eta_0 = 1$ crossover, increasing Γ_0 (by increasing $|\zeta|$) can push η_0 further below unity, causing the SLP to *decrease*, see results in Fig. 1. This nonmonotonic behavior is missed by the slow-relaxation approximation SLP $\approx (\mu_0/2\pi)\,H_0^2\,\chi_{\rm eq}\,\Gamma_0$ and is one of the central results of this work.

Since SA decreases $\chi_{\rm eq}$ but increases Γ_0, the net effect on the SLP depends on the competition between these two tendencies, mediated by the position of the system on the Debye curve. For sufficiently large σ and $\zeta > 0$, the relaxation rate dominates through barrier lowering [Eq. (13)], while for $\zeta < 0$ the enhancement enters through the algebraic prefactor.

3. Results and discussion

We compute the SLP for maghemite (γ-Fe_2O_3) nanoparticles of diameter $D = 12$ nm with a saturation magnetization of $M_{\rm s} = 4.8\times10^5$ A/m, an effective uniaxial anisotropy of $K_2 = 3\times10^4$ J/m^3, and at a temperature of $T = 300$ K. These parameters yield $\sigma \approx 6.6$. The AC field has a frequency of $f = 100$ kHz and an amplitude of $\mu_0 H_0 = 10$ mT. The damping parameter is set to $\lambda = 1$ and the attempt time to $\tau_0 = 10^{-9}$ s. A key quantity is the reduced frequency at $\zeta = 0$: for $\sigma = 7$ one finds $\eta_0 \equiv \omega/\Gamma_0 \approx 0.23$ (fast relaxation), while for $\sigma = 10$ and 15 one has $\eta_0 \approx 3.9$ and 470, respectively.

Fig. 1(a) displays the SLP, normalized to its value at $\zeta = 0$, as a function of ζ for three values of σ. The full Debye factor in Eq. (8) is used throughout. Several features emerge:

(i) The behavior of the SLP depends qualitatively on σ. For $\sigma = 15$ ($\eta_0 \approx 470$ at $\zeta = 0$, deep slow relaxation), the SLP is dramatically enhanced by surface anisotropy: at $\zeta = 0.2$ the SLP is roughly 5.5 times its $\zeta = 0$ value, rising to a factor of $\sim$14 at $\zeta = 0.5$. For $\sigma = 10$ ($\eta_0 \approx 3.9$), the enhancement is more modest, reaching a factor of $\sim$2 at $|\zeta| = 0.2$.

(ii) Strikingly, for $\sigma = 7$ ($\eta_0 \approx 0.23$, fast-relaxation regime), the SLP *decreases* with $|\zeta|$. This is because the system already lies below the peak of the Debye factor ($\eta_0 = 1$): increasing Γ_0 by surface anisotropy pushes η_0 further below unity, reducing χ''. This nonmonotonic σ-dependence is entirely absent from the slow-relaxation approximation and demonstrates the importance of retaining the full Debye factor.

(iii) The enhancement is *asymmetric* with respect to the sign of ζ. This asymmetry originates from the qualitatively different mechanisms at play for $\zeta > 0$ versus $\zeta < 0$ [Eq. (13)]. For $\zeta > 0$, which according to Yanes et al. [21] corresponds to particles with an fcc internal structure (where the surface-induced cubic anisotropy is positive), the energy barrier is reduced by $\sigma\zeta/4$, producing an exponential boost of the relaxation rate. For $\zeta < 0$, corresponding to sc-type particles [21], the energy barrier remains exactly equal to σ and the entire enhancement comes from the modification of the Kramers prefactor: the eigenvalues $\mu_{1,2}^{(\rm s)}$ at the saddle and the attempt frequency ν change with ζ, yielding a non-negligible (though algebraic rather than exponential) increase in Γ_0. We recall that the EOSP mapping becomes unreliable for $|\zeta|$ exceeding $\sim$0.25 on the sc lattice, whereas a wider range $|\zeta| \lesssim 0.35$ is accessible on the fcc lattice [21].

(iv) For large σ, the effect is more pronounced at higher σ: at $\sigma = 15$ the SLP ratio exceeds 14 for $\zeta = 0.5$. This is consistent with the exponential sensitivity of the relaxation rate to the energy barrier for $\zeta > 0$, $\Gamma_0 \propto \exp(-\sigma(1-\zeta/4))$: the amplification scales as $e^{\sigma\zeta/4}$, which is naturally more dramatic for larger σ. For $\zeta < 0$, the σ-dependence enters through the prefactor, which is a weaker (algebraic) effect.

The origin of the enhancement is elucidated in Fig. 1(b) and (c), which show the individual ζ-dependence of $\chi_{\rm eq}$ and Γ_0 at $\sigma = 10$. While $\chi_{\rm eq}$ decreases monotonically with ζ [Fig. 1(b)], the variation is only $\sim$5% over the range shown. In contrast, the relaxation rate [Fig. 1(c)]

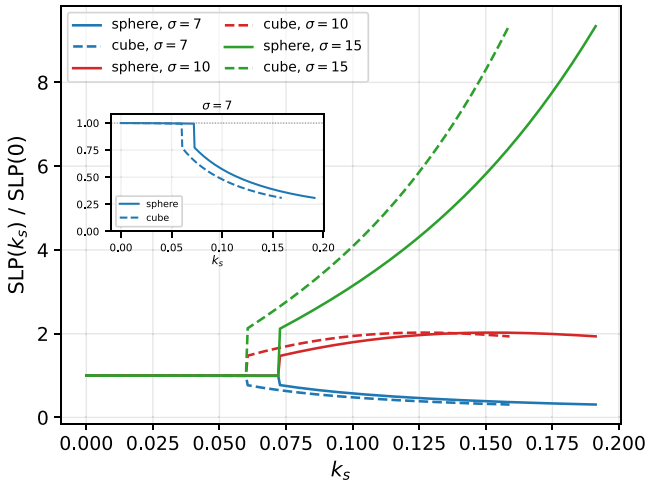

Fig. 2. Normalized SLP as a function of the dimensionless surface-anisotropy constant K_s for spherical (solid) and cubic (dashed) nanomagnets on an fcc lattice ($\zeta > 0$), for three values of σ. The inset magnifies the $\sigma = 7$ curves, showing the monotonic SLP decrease characteristic of the fast-relaxation regime. The effective cubic coefficient $k_4(K_s)$ is computed from Eq. (4): $k_4 = \kappa K_s^2/z$ for the sphere (with $\kappa = 0.535$) and $k_4 = (1 - 0.7/\mathcal{N}^{1/3})^4 K_s^2/z$ for the cube. Parameters: $\mathcal{N} = 1500$, $z = 12$ (fcc), $k_c = 0.01$, $N_c/\mathcal{N} \approx 0.47$. Curves are clipped at $\zeta = 0.35$ (EOSP validity limit).

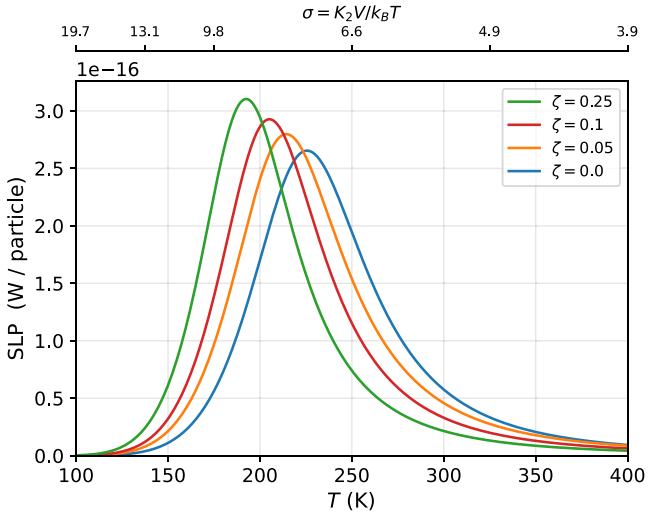

Fig. 3. SLP of a maghemite nanoparticle ($D = 12$ nm) as a function of temperature for several values of ζ (see inset). The top axis shows the corresponding reduced barrier $\sigma = K_2V/k_BT$. Parameters: $\lambda = 1$, $\tau_0 = 10^{-9}$ s, $f = 100$ kHz, $\mu_0 H_0 = 10$ mT.

increases by nearly an order of magnitude. Hence, for systems in the slow-relaxation regime, the SLP enhancement is overwhelmingly driven by the increase in the overbarrier switching rate.

Let us summarize the physical mechanism: the quartic anisotropy breaks the continuous azimuthal symmetry around the easy axis and creates discrete saddle points at the equator. For $\zeta > 0$, these additional escape routes lower the effective barrier, producing an exponential speedup of the thermally activated reversal. For $\zeta < 0$, the barrier height is unchanged but the curvatures at the saddle points are modified, increasing the attempt frequency and thus enhancing the reversal rate through the Kramers prefactor. In the context of hyperthermia, this means that nanomagnets with stronger surface effects dissipate energy more efficiently *provided* σ is large enough for the system to reside in the slow-relaxation regime ($\eta_0 > 1$). For smaller σ — i.e., near the superparamagnetic regime — the additional speedup of the relaxation can be counterproductive by pushing the system past the optimal $\eta_0 = 1$ condition. The underlying crystal structure matters: the results of Yanes et al. [21] imply that NPs with an fcc lattice (positive ζ) benefit from both barrier lowering and prefactor enhancement, while sc-lattice NPs (negative ζ) are enhanced only through the prefactor.

3.1. Shape dependence: sphere versus cube

The EOSP coefficient k_4 depends on the nanomagnet shape through Eq. (4). For a given value of the atomistic surface-anisotropy constant K_s, the cube yields a larger effective ζ than the sphere because $(1 - 0.7/\mathcal{N}^{1/3})^4 > \kappa$ for the particle sizes of interest. With $\mathcal{N} = 1500$ on an fcc lattice ($z = 12$) and $\kappa = 0.535$, the cube-to-sphere ratio is $(1 - 0.7/\mathcal{N}^{1/3})^4/\kappa \approx 1.45$.

Fig. 2 displays the normalized SLP as a function of K_s for both shapes and several values of σ. For $\sigma = 15$, the cube reaches an SLP enhancement of nearly an order of magnitude at $K_s \approx 0.15$, whereas the sphere achieves the same level of enhancement only at larger K_s. This difference is purely geometric in origin: the surface integral κ for the sphere is smaller than the corresponding prefactor for the cube, so that the cubic contribution to the effective anisotropy builds up more slowly with K_s. The cube also reaches the EOSP validity limit ($\zeta = 0.35$) at a smaller K_s (≈0.16) than the sphere (≈0.19). For $\sigma = 7$, both shapes show a decrease of the SLP with K_s, confirming the fast-relaxation suppression discussed above.

3.2. Temperature dependence of the SLP

Finally, we examine the temperature dependence of the SLP at fixed ζ. Since $\sigma = K_2V/(k_BT)$, varying T scans through both the slow- and fast-relaxation regimes. The SLP is expected to exhibit a maximum at the temperature T^* where $\eta_0 = \omega/\Gamma_0 \approx 1$, i.e., where the Debye dissipation is maximal.

Fig. 3 shows the SLP as a function of T for $\zeta = 0$, 0.05, 0.1, and 0.25. All curves display the expected bell shape. The peak shifts to lower temperature with increasing ζ: from $T^* \approx 225$ K ($\sigma \approx 8.7$) at $\zeta = 0$ to $T^* \approx 192$ K ($\sigma \approx 10.2$) at $\zeta = 0.25$. This shift is a direct consequence of the enhancement of Γ_0 by surface anisotropy, which pushes the $\eta_0 = 1$ crossover to higher σ (lower T). The peak amplitude increases modestly (~17% over the range of ζ shown), because at the Debye maximum the SLP reduces to $(\mu_0\omega/2\pi)\, H_0^2\, \chi_{eq}/2$, which depends only weakly on ζ through χ_{eq}. At temperatures above T^*, the system enters the fast-relaxation regime ($\eta_0 < 1$) and the SLP decreases; this is the regime in which further increasing Γ_0 through surface anisotropy becomes counterproductive, as discussed in Section 3.

4. Conclusion

We have presented a qualitative, semi-analytical study of how spin non-collinearities in nanomagnets affect the specific loss power (SLP) within the linear-response theory. By exploiting the analytical framework of the effective one-spin problem (EOSP) and focusing on the experimentally important case of surface-induced spin disorder, we have derived a semi-analytical expression for the SLP as a function of the surface-anisotropy parameter $\zeta = K_4/K_2$, the reduced energy barrier σ, and the damping parameter λ. A central result is the importance of the behavior of the Debye factor $\eta_0/(1+\eta_0^2)$: for systems in the slow-relaxation regime ($\eta_0 \gg 1$), the dominant mechanism is the increase of the relaxation rate Γ_0 caused by the creation of additional saddle points in the energy landscape, leading to an SLP enhancement. In contrast, for moderate σ values where $\eta_0 \lesssim 1$ (near the superparamagnetic regime), the same increase in Γ_0 can push the system past the optimal Debye condition, resulting in a *decrease* of the SLP. The sign of ζ, which is set by the underlying crystal lattice as established in Ref. [21], leads to quantitatively different barrier reductions and therefore to an asymmetric SLP enhancement. We have also shown that, for a

given surface-anisotropy constant K_s, the nanomagnet shape (sphere versus cube) modulates the effective ζ through the geometric prefactors in Eq. (4), with cubes producing a stronger SLP enhancement than spheres. The temperature dependence of the SLP exhibits a bell-shaped curve whose peak shifts to lower temperatures with increasing ζ.

We emphasize that the present analysis is restricted to relatively weak spin disorder, where the EOSP mapping onto a macroscopic potential with uniaxial and quartic terms remains valid. Stronger disruptions of the spin order — such as magnetic vortex states [26–28], spin frustration at interfaces, or spin textures induced by Dzyaloshinskii–Moriya exchange coupling [29,30] — can produce qualitatively similar but potentially much larger modifications of the effective energy landscape. Such situations lie beyond the scope of analytical approaches and require full numerical simulations of the many-spin problem [31]. A conceptually related but distinct problem is posed by strong, spatially uncorrelated anisotropy disorder in extended, exchange-coupled ferromagnets, where a scaling argument links the weak- and strong-disorder regimes and predicts a microwave-absorption band that saturates with spin heating at high power or temperature [33,34] — in contrast to the single-particle, coherent EOSP treatment developed here. We are currently extending the comparison to dipolar-interacting nanomagnet chains, where kinetic Monte Carlo simulations can be compared with analytical predictions. The qualitative trends identified here — the competition between barrier lowering and the Debye dissipation condition, the asymmetry with respect to the sign of the induced anisotropy, and the shape dependence — are expected to persist and to serve as guidelines for interpreting more complex numerical studies.

CRediT authorship contribution statement

A. Michels: Writing – review & editing, Validation, Investigation, Formal analysis, Conceptualization. **H. Kachkachi:** Writing – original draft, Supervision, Project administration, Methodology, Investigation, Formal analysis, Conceptualization.

Declaration of competing interest

The authors declare that they have no known competing financial interests or personal relationships that could have appeared to influence the work reported in this paper.

Data availability

No data was used for the research described in the article.

References

[1] J. Carrey, B. Mehdaoui, M. Respaud, Simple models for dynamic hysteresis loop calculations of magnetic single-domain nanoparticles: Application to magnetic hyperthermia optimization, J. Appl. Phys. 109 (8) (2011).

[2] B. Mehdaoui, A. Meffre, J. Carrey, S. Lachaize, L.-M. Lacroix, M. Gougeon, B. Chaudret, M. Respaud, Optimal size of nanoparticles for magnetic hyperthermia: A combined theoretical and experimental study, Adv. Funct. Mater. 21 (2011) 4573–4581.

[3] C. Haase, U. Nowak, Role of dipole–dipole interactions for hyperthermia heating of magnetic nanoparticle ensembles, Phys. Rev. B 85 (2012) 045435, http://dx.doi.org/10.1103/PhysRevB.85.045435, URL https://link.aps.org/doi/10.1103/PhysRevB.85.045435.

[4] C. Martinez-Boubeta, K. Simeonidis, A. Makridis, M. Angelakeris, O. Iglesias, P. Guardia, A. Cabot, L. Yedra, S. Estradé, F. Peiró, et al., Learning from nature to improve the heat generation of iron-oxide nanoparticles for magnetic hyperthermia applications, Sci. Rep. 3 (2013) 1652, http://dx.doi.org/10.1038/srep01652.

[5] I. Conde-Leboran, D. Baldomir, C. Martinez-Boubeta, O. Chubykalo-Fesenko, M. Puerto del Morales, G. Salas, D. Cabrera, J. Camarero, F.J. Teran, D. Serantes, A single picture explains diversity of hyperthermia response of magnetic nanoparticles, J. Phys. Chem. C 119 (27) (2015) 15698–15706, http://dx.doi.org/10.1021/acs.jpcc.5b02555.

[6] S. Ruta, R. Chantrell, O. Hovorka, Unified model of hyperthermia via hysteresis heating in systems of interacting magnetic nanoparticles, Sci. Rep. 5 (2015) 9090, http://dx.doi.org/10.1038/srep09090.

[7] R.E. Rosensweig, Heating magnetic fluid with alternating magnetic field, J. Magn. Magn. Mater. (ISSN: 0304-8853) 252 (2002) 370–374, URL http://www.sciencedirect.com/science/article/pii/S0304885302007060, Proceedings of the 9th International Conference on Magnetic Fluids, 23-27 Jul. 2001.

[8] R. Hergt, S. Dutz, R. Müller, M. Zeisberger, Magnetic particle hyperthermia: nanoparticle magnetism and materials development for cancer therapy, J. Phys. : Condens. Mater. 18 (2006) 2919, http://dx.doi.org/10.1088/0953-8984/18/38/S26.

[9] G. Barrera, P. Allia, P. Tiberto, Magnetic nanoparticle hyperthermia enhanced by a rotating field, Phys. Rev. Appl. 21 (2024) 064037, http://dx.doi.org/10.1103/PhysRevApplied.21.064037.

[10] D.P. Valdés, E. Lima Jr., R.D. Zysler, Theoretical investigation of nanoparticle relaxation for magnetic hyperthermia applications: Effects of size, anisotropy, and interparticle distance distributions, ACS Appl. Nano Mater. 8 (2025) 10663–10674, http://dx.doi.org/10.1021/acsanm.5c01608.

[11] N. Maniotis, M. Maragakis, N. Vordos, A comprehensive analysis of nanomagnetism models for the evaluation of particle energy in magnetic hyperthermia, Nanoscale Adv. 7 (2025) 4252–4269, http://dx.doi.org/10.1039/D5NA00258C.

[12] J.-L. Déjardin, F. Vernay, M. Respaud, H. Kachkachi, Effect of dipolar interactions and DC magnetic field on the specific absorption rate of an array of magnetic nanoparticles, J. Appl. Phys. 121 (20) (2017) 203903.

[13] G.T. Landi, F.R. Arantes, D.R. Cornejo, A.F. Bakuzis, I. Andreu, E. Natividad, AC susceptibility as a tool to probe the dipolar interaction in magnetic nanoparticles, J. Magn. Magn. Mater. (ISSN: 0304-8853) 421 (2017) 138–151, http://dx.doi.org/10.1016/j.jmmm.2016.08.011, URL http://www.sciencedirect.com/science/article/pii/S0304885316316559.

[14] Effects of surface anisotropy on hysteresis in fine magnetic particles, Phys. Rev. B 50 (1994) 3077.

[15] R.H. Kodama, A.E. Berkovitz, Atomic-scale magnetic modeling of oxide nanoparticles, Phys. Rev. B 59 (1999) 6321.

[16] H. Kachkachi, D.A. Garanin, Magnetic free energy at elevated temperatures and hysteresis of magnetic particles, Phys. A 291 (2001) 485.

[17] H. Kachkachi, D.A. Garanin, Spin-wave theory for finite classical magnets and superparamagnetic relation, Eur. Phys. J. B 22 (2001) 291–300, http://dx.doi.org/10.1007/s100510170106.

[18] O. Iglesias, A. Labarta, Finite-size and surface effects in maghemite nanoparticles: Monte Carlo simulations, Phys. Rev. B 63 (2001) 184416.

[19] Hysteretic properties of a magnetic particle with strong surface anisotropy, Phys. Rev. B 66 (2002) 174419.

[20] H. Kachkachi, D.A. Garanin, Magnetic nanoparticles as many-spin systems, in: D. Fiorani (Ed.), Surface Effects in Magnetic Nanoparticles, Springer, Berlin, 2005, p. 75.

[21] R. Yanes, O. Fesenko-Chubykalo, H. Kachkachi, D.A. Garanin, R. Evans, R.W. Chantrell, Effective anisotropies and energy barriers of magnetic nanoparticles within the néel's surface anisotropy, Phys. Rev. B 76 (064416) (2007).

[22] D.A. Garanin, H. Kachkachi, Surface contribution to the anisotropy of magnetic nanoparticles, Phys. Rev. Lett. 90 (065504) (2003) http://dx.doi.org/10.1103/PhysRevLett.90.065504, URL http://link.aps.org/doi/10.1103/PhysRevLett.90.065504.

[23] H. Kachkachi, Effects of spin non-collinearities in magnetic nanoparticles, J. Magn. Magn. Mater. 316 (248) (2007).

[24] D.A. Garanin, Effective anisotropy due to the surface of magnetic nanoparticles, Phys. Rev. B 98 (2018) (2018).

[25] A. Lappas, G. Antonaropoulos, K. Brintakis, M. Vasilakaki, K.N. Trohidou, V. Iannotti, G. Ausanio, A. Kostopoulou, M. Abeykoon, I.K. Robinson, E.S. Bozin, Vacancy-driven noncubic local structure and magnetic anisotropy tailoring in Fe_xO-$Fe_{3-\delta}O_4$ nanocrystals, Phys. Rev. X 9 (2019) 041044.

[26] T. Shinjo, T. Okuno, R. Hassdorf, K. Shigeto, T. Ono, Magnetic vortex core observation in circular dots of permalloy, Science 289 (2000) 930–932.

[27] N.A. Usov, M.S. Nesmeyanov, V.P. Tarasov, Magnetic vortices as efficient nano heaters in magnetic nanoparticle hyperthermia, Sci. Rep. 8 (2018) 1224.

[28] E.M. Jefremovas, L. Calus, J. Leliaert, Coercivity-size map of magnetic nanoflowers: Spin disorder tunes the vortex reversal mechanism and tailors the hyperthermia sweet spot, Small Sci. 6 (2026) e202500490, http://dx.doi.org/10.1002/smsc.202500490, URL https://onlinelibrary.wiley.com/doi/abs/10.1002/smsc.202500490.

[29] I. Dzyaloshinsky, J. Phys. Chem. Solids 4 (241) (1958).

[30] T. Moriya, Phys. Rev. 120 (1960) 91.

[31] O. Iglesias, H. Kachkachi, Single Nanomagnet Behaviour: Surface and Finite-Size Effects, Springer International Publishing, Cham, ISBN: 978-3-030-60473-8, 2021, pp. 3–38, http://dx.doi.org/10.1007/978-3-030-60473-8_1.

[32] D. Faílde, V. Ocampo-Zalvide, D. Serantes, Ò. Iglesias, Understanding magnetic hyperthermia performance within the "Brezovich criterion": beyond the uniaxial anisotropy description, Nanoscale 16 (2024) 14319–14329, http://dx.doi.org/10.1039/D4NR02045F.

[33] E.M. Chudnovsky, D.A. Garanin, Scaling theory of magnetic order and microwave absorption in amorphous and granular ferromagnets, Phys. Rev. B 109 (2024) 054429, http://dx.doi.org/10.1103/PhysRevB.109.054429.

[34] D.A. Garanin, E.M. Chudnovsky, Nonlinear and thermal effects in the absorption of microwaves by random-anisotropy magnets, Phys. Rev. B 105 (2022) 064402, http://dx.doi.org/10.1103/PhysRevB.105.064402.
[35] F. Vernay, Z. Sabsabi, H. Kachkachi, Phys. Rev. B 90 (094416) (2014).
[36] Surface-induced cubic anisotropy in nanomagnets, Phys. Rev. B 73 (2006) 224402.
[37] D.A. Garanin, Effective anisotropy due to the surface of magnetic nanoparticles, Phys. Rev. B 98 (2023) 054427.
[38] M.P. Adams, A. Michels, H. Kachkachi, Spatial magnetization profile in spherical nanomagnets with surface anisotropy: Green's function approach, Phys. Scr. 98 (2023) 105512.
[39] J.I. Gittleman, B. Abeles, S. Bozowski, Phys. Rev. B 9 (3891) (1974).
[40] M.I. Shliomis, V.I. Stepanov, J. Magn. Magn. Mater. 122 (176) (1993).
[41] J.L. Garcia-Palacios, On the Statics and Dynamics of Magnetoanisotropic Nanoparticles, Vol. 112, John Wiley & Sons, Inc, ISBN: 9780470141717, 2007, pp. 1–210, http://dx.doi.org/10.1002/9780470141717.ch1.
[42] Z. Sabsabi, F. Vernay, O. Iglesias, H. Kachkachi, Interplay between surface anisotropy and dipolar interactions in an assembly of nanomagnets, Phys. Rev. B 88 (2013) 104424.
[43] J.S. Langer, Theory of nucleation rates, Phys. Rev. Lett. 21 (1968) 973–976, http://dx.doi.org/10.1103/PhysRevLett.21.973, URL http://link.aps.org/doi/10.1103/PhysRevLett.21.973.
[44] J.S. Langer, Statistical theory of the decay of metastable states, Ann. Phys. (N. Y.) 54 (258) (1969).
[45] H.B. Braun, Kramers's rate theory, broken symmetries, and magnetization reversal, J. Appl. Phys. 76 (1994) 6310.
[46] H.B. Braun, Statistical mechanics of nonuniform magnetization reversal, Phys. Rev. B 50 (1994) 16501.
[47] H. Kachkachi, Effect of exchange interaction on superparamagnetic relaxation, Europhys. Lett. 62 (2003) 650.
[48] H. Kachkachi, Dynamics of a nanoparticle as a one-spin system and beyond, J. Mol. Liq. 114 (113) (2004).
[49] S. Titov, H. Kachkachi, Yu. Kalmykov, W.T. Coffey, Magnetization dynamics of two interacting spins in an external magnetic field, Phys. Rev. B 72 (134425) (2005).
[50] H. Kachkachi P.-M. Déjardin, Yu. Kalmykov, Thermal and surface anisotropy effects on the magnetization reversal of a nanocluster, J. Phys. D: Appl. Phys. 41 (2008) 134004.
[51] L. Néel, Théorie du trainage magnétique des substances massives dans le domaine de rayleigh, J. Phys. Radium 11 (1950) 49–61.
[52] W.F. Brown, Thermal fluctuations of a single-domain particle, Phys. Rev. 135 (1963) 1677.
[53] A. Aharoni, Effect of a magnetic field on the superparamagnetic relaxation time, Phys. Rev. 177 (1969) 793–796, http://dx.doi.org/10.1103/PhysRev.177.793, URL http://link.aps.org/doi/10.1103/PhysRev.177.793.
[54] J.C. Davidson, N.R. Anderson, K.L. Livesey, Field-dependent magnetic relaxation times of magnetic nanoparticle systems: Analytic approximations supported by numerical simulations, Phys. Rev. B 110 (2024) 144447, http://dx.doi.org/10.1103/PhysRevB.110.144447.